Probing Electric and Magnetic Fields with a Moiré Deflectometer

P. Lansonneur[a,*], P. Bräunig[b], A. Demetrio[b], S. R. Müller[b], P. Nedelec[a], M. K. Oberthaler[b]

[a] *Institut de Physique Nucléaire de Lyon, CNRS/IN2P3, 69622 Villeurbanne, France*
[b] *Kirchhoff-Institut für Physik, Heidelberg University, Im Neuenheimer Feld 227, 69120 Heidelberg, Germany*

Abstract

A new contact-free approach for measuring simultaneaously electric and magnetic field is reported, which considers the use of a low energy ion source, a set of three transmission gratings and a position sensitive detector. Recently tested with antiprotons [1] at the CERN Antiproton Decelerator facility, this paper extends the proof of principle of a moiré deflectometer [2] for distinguishing electric from magnetic fields and opens the route to precision measurements when one is not limited by the ion source intensity. The apparatus presented, whose resolution is mainly limited by the shot noise is able to measure fields as low as $9\,\mathrm{mV\,m^{-1}\,Hz^{-1/2}}$ for electric component and $100\,\mathrm{\mu G\,Hz^{-1/2}}$ for the magnetic component. Scaled to 100 nm pitch for the gratings, accessible with current state-of-the-art technology [3], the moiré fieldmeter would be able to measure fields as low as $22\ \mathrm{\mu V\,m^{-1}\,Hz^{-1/2}}$ and $0.2\ \mathrm{\mu G\,Hz^{-1/2}}$.

Keywords: Fieldmeter, Lorentz force, Moiré effect

1. Introduction

Depending on the frequency range considered, electric field meters usually rely on different operating principles. Antennas reach the best performances to measure time-varying electric fields, when frequencies typically overcome 100 kHz. Reference [4] gives the example of a dipolar double probe, able to measure electric fields with a sensitivity of $E_{\mathrm{min}} = 1\,\mathrm{mV\,m^{-1}}$ at several MHz. Instead, the highest sensitivities for static or low-frequency electric fields are achieved with “voltmeter-type” sensors where the potential difference between two plates placed apart is precisely measured. Krupka et al. [5] reports for instance a sensitivity of $2\,\mathrm{\mu V\,m^{-1}\,Hz^{-1/2}}$ at 100 Hz with plates placed 33 cm apart. Although those devices show a high sensitivity, the field magnitude is indirectly evaluated by the amount of charges it induces.

Another category of apparatus builds on free charges in vacuum. The use of particle beams, combined with a position sensitive detector, allows to perform precise contact-free measurements over large experimental volumes and to probe directly the field itself. The steered electron field sensor [6], in which two anodes measures the shift induced by an external electric field on an electron beam, is for example able to resolve a field of $34\,\mathrm{mV\,m^{-1}\,Hz^{-1/2}}$ at 10 Hz. In its current state, such a device is however not able to determine if the shift measured is due to an electric or a magnetic field. A similar approach is here reported, which presents the advantage of distinguishing the electric from the magnetic field component with the same device.

2. Moiré Fieldmeter

2.1. Moiré principle

The principle of the moiré fieldmeter can be seen as an extension of the simple setup depicted in figure 1(a) In this configuration, a non-collimated beam passes through two apertures separated by a distance L, which constrain the trajectories of the particles reaching the detector. Undeflected particles such as neutral atoms conserve straight trajectories throughout the whole apparatus while particles submitted to a force will experience an acceleration in the vertical direction leading to a parabolic trajectory. The shift Δy between the two

*Corresponding author
Email address: fieldmeter@matterwave.de

impacts on the position sensitive detector is given by $\Delta y = a\tau^2$ where a is the acceleration in the direction orthogonal to the slits and $\tau = L/v_z$ is the time of flight between the two slits.

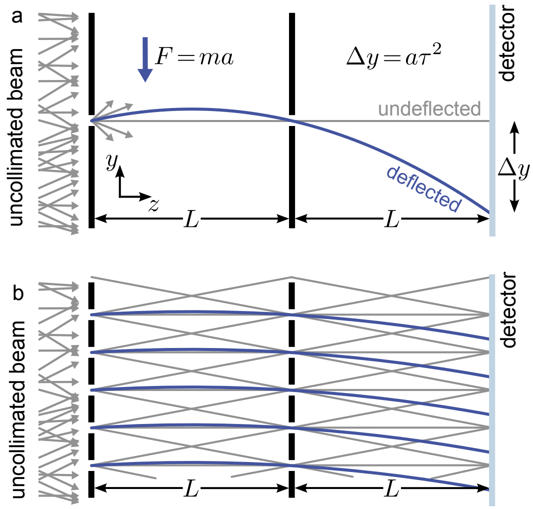

Figure 1: a) Two slits separated by a distance L restrict the path of a beam to a specific trajectory. b) Replacing the slits by two gratings increases the flux of particles reaching the detector. Since the first grating constrains the ions trajectories, the moiré device does not require the beam to be collimated (image from [7]).

If the two slits are replaced by two gratings having a certain periodicity d, the pattern seen on the detector plane becomes a collection of fringes with same periodicity as the gratings (figure 1(b)). The moiré fieldmeter gives hence a measurement of the field, assumed homogeneous, over the whole length of the apparatus. It can be particularly beneficial for experiments dealing with fields which needs to be controlled over large volumes. Observing such a pattern can however be problematic if the slits separation gets smaller than the detector resolution. Adding a third grating with the same periodicity as the first two, but tilted by a small angle, allows to take advantage of the moiré effect to reveal macroscopic fringes orthogonal to the slit orientation as shown in figure 2.

For a small angle between the gratings, the macroscopic fringes periodicity D is directly proportional to the gratings pitch and scales with the inverse of the angle α such that $D = d/\sin\alpha$. The visibility $\nu = (\mathrm{I}_{\max} - \mathrm{I}_{\min})/(\mathrm{I}_{\max} + \mathrm{I}_{\min})$ of the macroscopic pattern formed depends on the open fraction of the gratings used. It is equal to 1 for

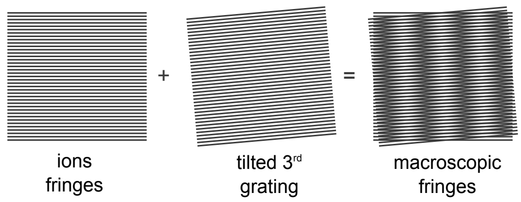

Figure 2: A third tilted grating placed behind the fringes but tilted by a small angle allows one to take advantage of the moiré effect to reveal a macroscopic pattern orthogonal to the slit orientation.

open fraction until 25 % and then drops rapidly to zero for 50 % open fraction, when the slits is exactly half of the grating periodicity. More details about the moiré principles can be found in reference [2].

2.2. *Decoupling magnetic and electric components*

When affected by both an electric and a magnetic field, charged particles experience Lorentz forces, translating into an acceleration $a = \frac{q}{m}|\vec{E} + \vec{v} \wedge \vec{B}|$. Following the axis convention of figure 1, and for small radial velocities[1], the field components leading to a shift along the y axis are trivially the components along y for $\vec{E}$ and along x for $\vec{B}$. Introducing V_{acc} the acceleration voltage of the ions (leading to an energy $q \cdot V_{\mathrm{acc}}$), the shift due to the Lorentz force writes:

$$\Delta y = \frac{L^2}{2V_{\mathrm{acc}}} E_y + \sqrt{\frac{q}{mV_{\mathrm{acc}}}} L^2 B_x. \qquad (1)$$

The knowledge of Δy for two different acceleration voltages or two different ion species (with distinct charge-to-mass ratios) leads therefore to a system of linear equations with a unique solution in E_y and B_x. Since neutral particles do not experience any force when placed in constant electric and magnetic fields, they are used to create a reference pattern. This extends the measurement of reference [1], where only the magnitude of the force is measured without probing its nature.

2.3. *Resolution limit*

The determination of the phase shift between the deflected particles and the neutral reference is depicted schematically in figure 3. Following the mathematical treatment given in reference [7], any

[1] such that $v_x \cdot B_z$ becomes negligible in comparison with $v_z \cdot B_x$.

phase shift measured on the detector is limited statistically by the shot-noise leading to an uncertainty proportional to $1/\sqrt{N}$.

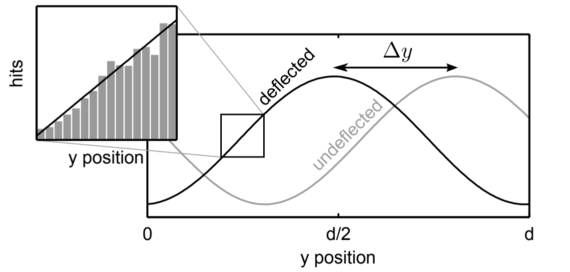

Figure 3: The fringe pattern is shifted by Δy due to an uniform acceleration (image from [7]).

The minimal detectable shift is expressed as:

$$\Delta y_{\min} = \frac{d}{2\pi\nu\sqrt{N}}, \tag{2}$$

where ν is the fringes visibility, d the grating periodicity and N the number of particles detected. By using equation (2), the minimal detectable electric field writes:

$$\begin{aligned} E_{\min} &= \frac{dV_{\mathrm{acc}}}{\pi\nu L^2\sqrt{N}}, \\ B_{\min} &= \frac{d}{2\pi\nu L^2\sqrt{N}}\sqrt{\frac{mV_{\mathrm{acc}}}{q}}. \end{aligned} \tag{3}$$

For a visibility of 1, a typical ion flux of 0.1 pA (corresponding to 10 000 particles detected per second) and a 171 mm distance between the gratings, the minimal field detectable with 2 keV ions is $9\,\mathrm{mV\,m^{-1}\,Hz^{-1/2}}$ and $100\,\mathrm{\mu G\,Hz^{-1/2}}$ for the magnetic field. For a given geometry of the grating, the visibility is also sensitive to the velocity distribution of the beam, affecting the resolution limit of the fieldmeter. Indeed, in the presence of any force, slow particles experience bigger deviations than fast ones. As a consequence, the fringes minima and maxima can possibly overlap such that the patterns smears out. One should notice that the detector resolution affects also the fringe visibility through the uncertainty it causes on each particle impact's coordinates. Convolving the fringes pattern with a gaussian distribution, we estimate the visibility to decrease by 20 % for a resolution as high as 10 % of the periodicity.

2.4. Field corrective factor

Because of its metallic parts, the moiré deflectometer bends the field lines when placed inside a uniform electric field. As a consequence, the field magnitude between the gratings gets effectively smaller. The correcting factor f accounts for this diminution. From Finite Elements Method simulation, we estimate this factor to be of the order of $f = 0.87$ for a setup consisting of only three free-standing gratings (assuming for instance that the gratings mechanical supports are made of a material with small permittivity ($\varepsilon_R \simeq 1$)). A view of the electric field distribution around the gratings and its evolution (for the vertical component) along a line going through the centre of the deflectometer (dashed line) are shown in the figure 4. The simulation is done with SIMION 8.0 [8] for an ambient field of $1\,\mathrm{V\,m^{-1}}$.

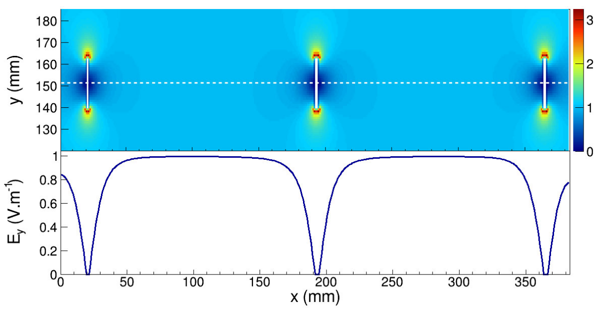

Figure 4: (top) Electric field distribution simulated with SIMION 8.0 [8] for an ambient field of $1\,\mathrm{V\,m^{-1}}$. The field magnitude gets higher around the gratings edges. (bottom) Profile of the vertical component of the field along the axis of the deflectometer (white dashed line on the top picture).

2.5. Maximal operating frequency

Assuming a readout fast enough for the imaging detector, the moiré fieldmeter is in principle not limited to static fields. In our setup, the maximal operating frequency is however imposed by the time of flight of the protons along the deflectometer. For 2 keV protons and $L = 171\,\mathrm{mm}$, the time of flight between the first and the third grating is $\Delta t = 276\,\mathrm{ns}$, corresponding to a maximal frequency of $1.8\,\mathrm{MHz}$.

3. Experimental Implementation

3.1. Setup

A schematic view of the system is shown in figure 5. The beam is exiting an Electron Cyclotron Resonance (ECR) ion source able to produce protons, H_2^+ and H_3^+ ions distinguished by the use of a Wien Filter. Its energy can be tuned from 500 eV to 2 keV and the intensity delivered ranges from few nA to less than 1 pA. The energy spread of the beam measured at the entrance of the fieldmeter is typically of the order of 1 to 2 %. More details on the source can be found in reference [9]. A nitrogen gas target placed right behind the source allows one to select either ions or hydrogen atoms formed by electron capture by tuning the pressure from 10^{-9} to 10^{-3} mbar.

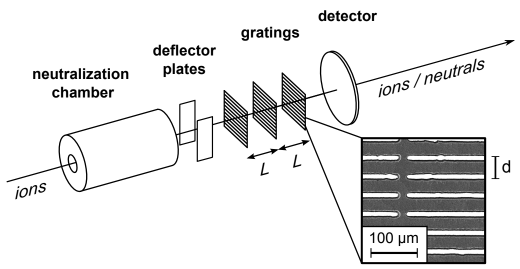

Figure 5: Schematic view of the experimental setup. The ions are sent through three transmission gratings and reach an imaging detector. For referencing purposes, a gas target and a set of deflector plates placed downstream enables one to switch from ion beam to neutral beam. The close-up shows a Scanning Electron Microscopy picture of the gratings.

By doing so, one benefits from an inline neutral beam for calibrating the fieldmeter. A set of two electrostatic deflector plates is used to eliminate the eventual remaining ions when neutral particles are selected. The beam is sent through three metal-coated silicon gratings with 40 µm periodicity with an open fraction of the order of 20 %, and spaced by a distance which may be tuned between 34 mm and 171 mm. Each grating is 10×10 mm^2 with a thickness of 100 µm and is mounted on vacuum compatible piezo actuators, allowing rotation (with millidegree resolution) around the beam axis for the two first ones. To avoid the slits to collapse on themselves, support structures are added to the gratings during the etching process. They consist in structures oriented perpendicularly to the slits and with periodicity ranging from one to several millimeters depending on each grating. Finally, a 25 mm in diameter Micro Channel Plate (MCP) with 12 µm channel size stacked to a resistive anode detects the particles outcoming the gratings.

3.2. Pattern reconstruction

The two-stages MCP amplifies the signal for each hit with a typical gain around 2.10^6. The Quantar Technology 3390A Resistive Anode Encoder [11] (RAE) converts then the analog signals to a set of digital coordinates stored in a 256 × 256 pixels matrix. The spatial resolution is of this model is of the order of 250 µm with typical background count rate of 5 per second [11]. For each ions species considered, the images are acquired with a flux of approximately 1 kHz during 1 min such than 10^4 to 10^5 events are taken into account in average. To minimize the effect of the non-uniformity of the detector (dead and hot stripes), the RAE is rotated with respect to the expected fringes orientation. Figure 6 shows a typical image of the moiré fringes, with a visibility of 0.92, obtained with neutral hydrogen.

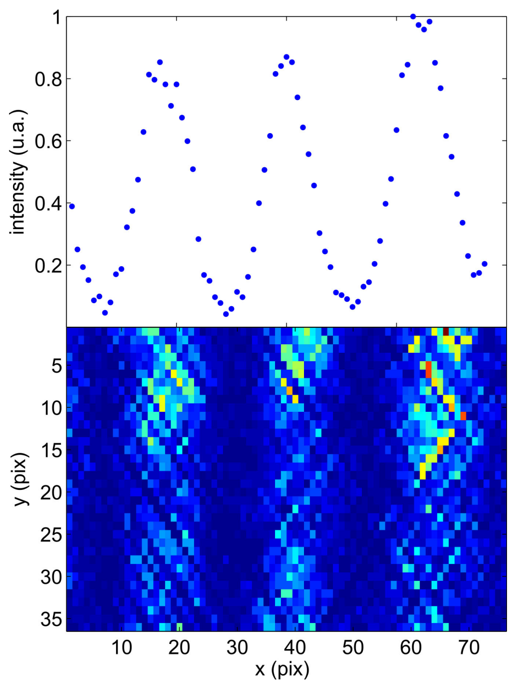

Figure 6: View of the moiré fringes obtained with neutral hydrogen on the resistive anode detector. The upper part plot represents the projection with a high visibility of 0.92. Such a pattern is used as a reference for measuring the shift difference between the ions.

3.3. Phase difference measurement

The pattern formed is then fitted by the function[2]

$$I(y) = \frac{a_0}{2} + \sum_{n=1}^{+\infty} a_n \cos(\frac{2\pi n}{d}(y+\phi)), \qquad (4)$$

where the a_n coefficients are given by:

$$a_n = 4\eta^3 \mathrm{sinc}^3(\pi\eta \mathrm{n})\cos(\pi\eta \mathrm{n}) \quad \forall \mathrm{n} \in \mathbb{N}, \qquad (5)$$

standing for the convolution of the last grating's transmission function with the projection of the second grating's pattern with open fraction η. As the Fourier coefficients get rapidly negligible [12], only the first ones (until $\mathrm{n} \leq 2$) are taken into account in the fit.

The field measurement is performed inside a three layers mu-metal magnetic shield with a shielding factor around 1000. The shield, also operating as a Faraday cage, guarantees a magnetic field below 20 mG and $10\,\mathrm{V\,m^{-1}}$ for the electric field. The moiré patterns for neutral hydrogen, protons, H_2^+ and H_3^+ ions at 2000 eV and for a distance of 171 mm between the gratings are plotted in figure 7. Although the total number of particles detected for each pattern is of the order of 10^4, fluctuations due to the RAE response can still be seen on the profiles. The corresponding shifts, scaled down to the original 40 µm periodicity of the gratings, are listed in table 1. The fit uncertainties originate from the non uniformity of the detector response and the 2.3 µm error on the pattern periodicity.

	shift Δy (µm)	error (µm)
protons	1.98	0.37
H_2^+	1.35	0.26
H_3^+	1.14	0.23

Table 1: Measured shift of the fringe pattern for H_3^+, H_2^+ ions and protons.

Considering each combinations of ion species (proton with H_2^+, proton with H_3^+ and H_2^+ with H_3^+) leads to three distinct measurements for the electric and magnetic fields following the equation system (1). Taking their mean values leads to:

$$\begin{aligned} E &= 0.91 \pm 0.31\ \mathrm{V\,m^{-1}} \\ B &= -15.2 \pm 6.8\ \mathrm{mG} \end{aligned} \qquad (6)$$

[2]The detailed mathematical treatment to obtain the Fourier decomposition can be found in reference [12].

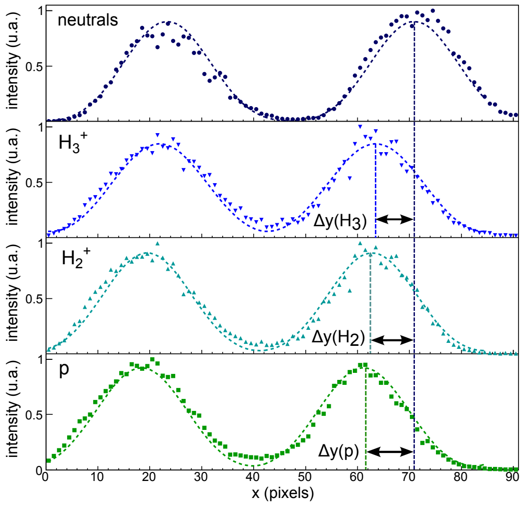

Figure 7: Moiré patterns for (from top to bottom) hydrogen, H_3^+, H_2^+ ions and protons. One can notice the spatial shift between the three species, listed in table 1. Measuring those shifts enables one to evaluate the magnitude of the fields acting on the ions.

where the errors originate from the standard deviation of the different combinations.

3.4. Test of the fieldmeter

The reliability of the fieldmeter is now evaluated with an homogeneous and known magnetic field. To do so, the three gratings, spaced here by 34 mm, are placed between two large rectangular Helmholtz coils with dimensions 500 × 280 mm, ensuring a uniform magnetic field (within 1 % based on Biot-Savart calculation [13]) between the gratings. As the distance between the gratings is strongly reduced to guarantee the magnetic field homogeneity, the sensitivity of the apparatus decreases quadratically to 2.4 $\mathrm{mG\,Hz^{-1/2}}$. A reference picture of the fringes is taken with neutral particles and for each current value, the shift Δy for 2 keV protons, H_2^+ and H_3^+ ions are obtained as in the previous section. The x-component of the magnetic field is independently measured with a Hall probe placed in the vicinity of the gratings.

The evolution of the magnetic and electric fields measured by the moiré fieldmeter as a function of the coil current I is given in figure 8. An affine function with a slope of 2.97 G/A is fitted to the data and compared to the Hall probe output (3.01 ± 0.07 G/A). Although the slopes are compatible, a 410 mG offset is measured between the

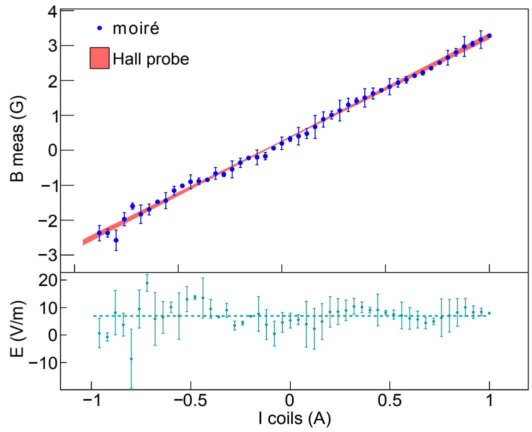

Figure 8: Measured electric and magnetic fields as a function of the coils current. The magnetic field, evaluated separately by a Hall probe, shows a linear dependency while the electric field remains constant of the order of 6.96 $\mathrm{V\,m^{-1}}$. On the upper plot, an offset field of 410 mG is added to the Hall probe response.

two devices. The difference is imputed to the improper nulling of the Hall sensor, while the moiré is calibrated “in absolute”by the neutrals and at the position of interest (in situ). One can notice on the other hand the stability of the electric field with the coil current.

4. Discussion

4.1. Charge-up effects

The strength of the moiré deflectometer as a fieldmeter relies on the fact that it does not create its own field. For this reason, every metallic part is grounded and the gratings, made of silicon, are metalized by an alloy of gold and palladium. The stability of the coating has been tested under the SEM microscope after one week of irradiation. For the intensity of ions considered (at most at the level of I = 1 pA), the stray resistance between the gratings and their support, of the order of a few ohms, can be responsible of an electric field at worst at the level of $R \cdot I/d \simeq \mathrm{\mu V\,m^{-1}\,Hz^{-1/2}}$, negligible for the sensitivity achieved. Reference [14] gives a picture illustrating how a local potential, a wire kept at a few volts, distorts Talbot-Lau Electron fringes.

4.2. Ions monochromaticity and visibility drop

For the energy spread considered, one can calculate the field leading to an overlap of the patterns created by the fastest and slowest ions. The worst case being when the two populations presents a phase shift of half a period, leading to a zero visibility. For a given energy spread ΔV_{acc}, the patterns generated by slow and fast particles are separated by $d/2$ when the critical electric field E_c is applied, such that:

$$\begin{cases} \Delta y = \dfrac{L^2}{2V_{\mathrm{acc}}} E_c \\ \Delta y + \dfrac{d}{2} = \dfrac{L^2}{2(V_{\mathrm{acc}} + \Delta V_{\mathrm{acc}})} E_c. \end{cases} \tag{7}$$

Solving this equation system allows one to retrieve the expression of the critical fields, which defines the robustness of the moiré fieldmeter. These equations can be translated into the following expressions for the critical magnetic and electric fields:

$$\begin{aligned} E_c &= \frac{dV_{\mathrm{acc}}^2}{L^2 \Delta V_{\mathrm{acc}}}, \\ B_c &= \frac{d}{L^2}\sqrt{\frac{m}{q}}\frac{V_{\mathrm{acc}}^{3/2}}{\Delta V_{\mathrm{acc}}}. \end{aligned} \tag{8}$$

For a 2 keV proton beam with 1 % energy spread and $L = 171$ mm, it corresponds to $E_c = 273\ \mathrm{V\,m^{-1}}$ and $B_c = 6.3$ G.

4.3. Absolute measurement and phase shift uncertainty

As any phase difference is measured modulo 2π, the phase shift considered between the two patterns is subject to an ambiguity (there is no way to distinguish a certain shift from the same shift modulo the pattern's period). It defines therefore the range of the field that can be measured by the moiré fieldmeter, dependent on the grating periodicity. From equation (1), this is expressed as:

$$\begin{aligned} \Delta E_y &= \frac{2dV_{\mathrm{acc}}}{L^2}, \\ \Delta B_x &= \frac{d}{L^2}\sqrt{\frac{mV_{\mathrm{acc}}}{q}}. \end{aligned} \tag{9}$$

For 2 keV ions and a pitch of $d = 40$ µm, it corresponds to 5.5 $\mathrm{V\,m^{-1}}$ and 63 mG for $L = 171$ mm (35 $\mathrm{V\,m^{-1}}$ and 1.6 G for $L = 34$ mm). In practice, the moiré fieldmeter is therefore a fine measurement device which needs to be associated to a standard field meter giving the order of magnitude.

5. Conclusion

A new method for measuring simultaneously electric and magnetic fields has been presented. A sensitivity of 9 $\mathrm{mV\,m^{-1}\,Hz^{-1/2}}$ and 100 $\mathrm{\mu G\,Hz^{-1/2}}$ has been achieved with a low-energy ion source delivering typically 10^7 particles per second, a set of three transmission gratings with 40 µm periodicity and a resistive anode detector. The monochromaticity of the ion source allows the device to measure fields until $E_c = 273\ \mathrm{V\,m^{-1}}$ and $B_c = 6.3$ G. Higher performances can be in principle achieved with gratings having sub-micron pitches. For 100 nm periodicity transmission gratings as the one used in reference [3], the moiré fieldmeter would be able to measure fields as low as 22 $\mathrm{\mu V\,m^{-1}\,Hz^{-1/2}}$ and 0.2 $\mathrm{\mu G\,Hz^{-1/2}}$ under the same conditions.

6. Acknowledgements

The authors express their grateful thanks to A. Kast, L. Veith and Pr. R. Schröder for their help with the gratings metalization and SEM images, and to iX-factory GmbH [15] for the gratings production. This work was supported by the PALSE mobility program from the PHAST doctoral school and the Deutsche Forschungsgemeinschaft [research grant no. OB164/10-1].

[1] S. Aghion et al., A moiré deflectometer for antimatter. Nature communications, 5 (2014) 1-6.

[2] M. K. Oberthaler, S. Bernet, E. M. Rasel, J. Schmiedmayer, and A. Zeilinger, Inertial sensing with classical atomic beams, Physical Review A, vol. 54, 4 (1996) 3166-3167.

[3] R. E. Grisenti, W. Schöllkopf, J.P. Toennies, J. R. Manson, T. A. Savas, & H. I. Smith, He-atom diffraction from nanostructure transmission gratings: The role of imperfections, Physical Review A, 61(3) (2000) 033608.

[4] R. L. Stenzel, A new probe for measuring small electric fields in plasmas. Review of scientific instruments, 62(1) (1991) 130-139.

[5] M. A. Krupka, R. Matthews, C. Say, A.D. Hibbs & G. D. Delory, Development and test of free space electric field sensors with microvolt sensitivity, Quantum Applied Science and Research Inc. San Diego CA, 2001.

[6] K. R. Williams, D. P. De Bruyker, S. J. Limb, E. M. Amendt & D. A. Overland, Vacuum steered-electron electric-field sensor, Journal of Microelectromechanical Systems, 23(1) (2014) 157-167.

[7] P. Bräunig, Atom Optical Tools for Antimatter Experiments, Heidelberg University PhD thesis, 2015.

[8] www.simion.com (accessed on January 1st, 2017)

[9] P. Sortais, T. Lamy, J. Médard, J. Angot, L. Latrasse & T. Thuillier, Ultracompact/ultralow power electron cyclotron resonance ion source for multipurpose applications, Review of Scientific Instruments, 81(2) (2010) 02B314.

[10] F. C. Haupert, A Moiré-Deflectometer as Gravimeter for Antihydrogen, Heidelberg University PhD thesis, 2012.

[11] http://www.quantar.com/pages/QTI/ofs.htm (accessed on January 1st, 2017)

[12] F. Bergermann, Characterization of the Moiré Deflectometer for the AEgIS-Experiment, Heidelberg University Diploma thesis, 2012.

[13] S. R. Müller, Moiré Deflectometer for Charged Particles, Heidelberg University Master thesis, 2015.

[14] A. D. Cronin, & B. McMorran, Electron interferometry with nanogratings, Physical Review A, 74(6) (2006) 061602.

[15] http://ix-factory.de/ (accessed on January 1st, 2017)